Supplementary Material for:
Iron and carbon isotope evidence for ecosystem and environmental diversity in the ~2.7 to 2.5 Ga Hamersley Province, Western Australia

Andrew D. Czaja, Clark M. Johnson, Brian L. Beard, Jennifer L. Eigenbrode, Katherine H. Freeman, Kosei E. Yamaguchi

S1. Geologic Setting

S1.1 Depositional environments

The depositional environments and geologic evolution of the main outcrop area have been described in detail by numerous workers (e.g., Trendall and Blockley, 1970; Davy and Hickman, 1988; Buick, 1992; Simonson et al., 1993; Thorne and Trendall, 2001; Barley et al., 2005). Additionally, Eigenbrode and Freeman (2006) described these environments based on the specific cores studied here. The oldest samples investigated here are from the Tumbiana Formation, which records mixed clastic deposition and carbonate precipitation, including numerous stromatolites, in a very shallow water environment of lacustrine or marine affinity (Buick, 1992; Sakurai et al., 2005; Eigenbrode and Freeman, 2006). The Tumbiana Formation is overlain by subaerial volcanic rocks of the Maddina Basalt (Thorne and Trendall, 2001), followed by the Jeerinah Formation, which records dominantly shallow water deposition at the base, followed by progressively deeper deposition upwards into fine-grained pyritic black shales (Thorne and Trendall, 2001). At the top of the Jeerinah Formation, continuing up into the Marra Mamba Iron Formation (IF), the depositional environment was relatively deep (below storm wave base), as recorded by finely laminated shales and iron formation (Trendall and Blockley, 1970; Morris, 1993). Marra Mamba IF deposition is interpreted to record volcanic activity, which increased Fe^{2+}_{aq} contents in the paleobasin and supplied tuffaceous material (Davy and Hickman, 1988; Morris, 1993). The transition from the Marra Mamba IF to the Wittenoom Formation reflects a shallowing upward succession and an increase in carbonate abundance in the form of turbidites that flowed basinward off of a shelf carbonate platform in the northeastern part of the province, followed by deposition on a ramp below storm wave base (Simonson et al., 1993; Simonson and Carney, 1999).

The depositional environment of the Oakover River area in the east-northeast part of the Hamersley Province has been described by Simonson et al. (1993), Eigenbrode and Freeman (2006), and Williams (2007). The Jeerinah Formation in this area (formerly called the Lewin Shale) was deposited in an environment similar to that of the Jeerinah Formation in the main outcrop area (Thorne and Trendall, 2001). The transition from the Jeerinah Formation to the Carawine Dolomite in the Oakover River area records shallowing upward deposition, but contrasts to the Jeerinah–Marra Mamba–Wittenoom succession in that below-storm-wave base pyritic black shales grade into slope deposits at the top of the Jeerinah Formation and base of the Carawine Dolomite before shifting to consistent carbonate platform deposition (Simonson et al., 1993). The Carawine platform is characterized by abundant stromatolites, indicating photic zone depths, and areas of organic- and carbonate-rich shale deposition indicative of locally restricted circulation on parts of the platform (Eigenbrode and Freeman, 2006).

S1.2 Geochronology

The cores from which samples were collected (WRL1, SV1 and RHDH2a) come from two regions of the Hamersley Province (see Fig. 1 in the main text). WRL1 and SV1 were

recovered from near the center of the paleobasin in what is called the "main outcrop area" (the WRL1 core was drilled at the depocenter (Meakins, 1987) and SV1 ~60 km to the NNW). RHDH2a was recovered from the east-northeast part of the province in the Oakover River area. These two regions of the province can be stratigraphically correlated by a single impact layer common to each (see below). Therefore, we developed a chronostratigraphic model to correlate our samples across ~300 km of the province.

Our chronostratigraphic model (Fig. S1) for the WRL1 and SV1 cores is based on that of Trendall et al. (2004), who produced a composite stratigraphic column using interpolated dates for the boundaries of each of the geologic units in the main outcrop area based on U–Pb ages and integrated depositional rates for the various lithologies. Our depositional rates differ somewhat from those of Trendall et al. (2004) because the thickness of each unit in the cores analyzed in our study differed from the idealized column they compiled. The boundaries and thickness of each unit within the WRL1 and SV1 cores were determined by Meakins (1987) and Richards (1985), respectively, who originally logged the cores, and by Eigenbrode and Freeman (2006) who collected the samples studied here.

The geochronology of the Oakover River area is not as well constrained because it has fewer outcrops and drill cores, and thus has not been as well documented as the main outcrop area in terms of geology, stratigraphy, and geochronology. To our knowledge, only one U–Pb age is known from this region, obtained from a tuff bed in the Carawine Dolomite, at 2630 ± 6 Ma (Rasmussen et al., 2005). This tuff layer is ~30 meters below a layer of impact spherules known as the Carawine impact layer. The age of this impact layer, as well as the spherule textures, match very nearly the age (2629 ± 5 Ma, Trendall et al., 2004) and textures (Hassler et al., 2005) of the spherules of the Jeerinah impact layer in the main outcrop area, and thus these layers are considered to have formed in the same impact event (Hassler et al., 2005; Rasmussen et al., 2005). The lack of other ages from this region requires the use of depositional rates to determine the relative ages of the various sample depths from within the core. Trendall et al. (2004) developed a model of depositional rates for various types of lithologies in the region. We have used their rates of 13 and 6 $m \cdot m.y^{-1}$. for carbonates and shales, respectively, to determine the relative ages of our samples from the Carawine Dolomite and Jeerinah Formation (Fig. S1, and Fig. 2 in the main text). Although such depositional rates are approximate and represent gross averages, reasonable adjustments to either of these values do not alter our conclusions.

S2. Sample preparation

Core samples were cut using a water-cooled rock saw and then the surfaces were hand sanded to remove any metal marks left by the saw blade. The samples were either crushed in a tungsten carbide piston press or placed in plastic sample bags and crushed by use of a rock hammer, which reduced the samples to fragments less than 10 millimeters in dimension. The crushed samples were rinsed 2 to 3 times with distilled deionized water (18.2 MΩ) to remove most of the allocthonous dust and then washed in an ultrasonic bath in distilled deionized water to remove any remaining dust. Finally, each sample was cleaned with acetone in an ultrasonic bath to remove any water and surficial organic contamination. Prior to milling, samples were stored in glass sample vials that had been cleaned with absolute ethanol. Most of the samples were powdered in a tungsten carbide ball mill (SPEX SamplePrep 8000) for 5 to 10 minutes. Those samples that were too small to pulverize in the ball mill (<3 g) were pulverized manually using an alumina mortar and pestle. All powdered samples were stored in clean glass vials.

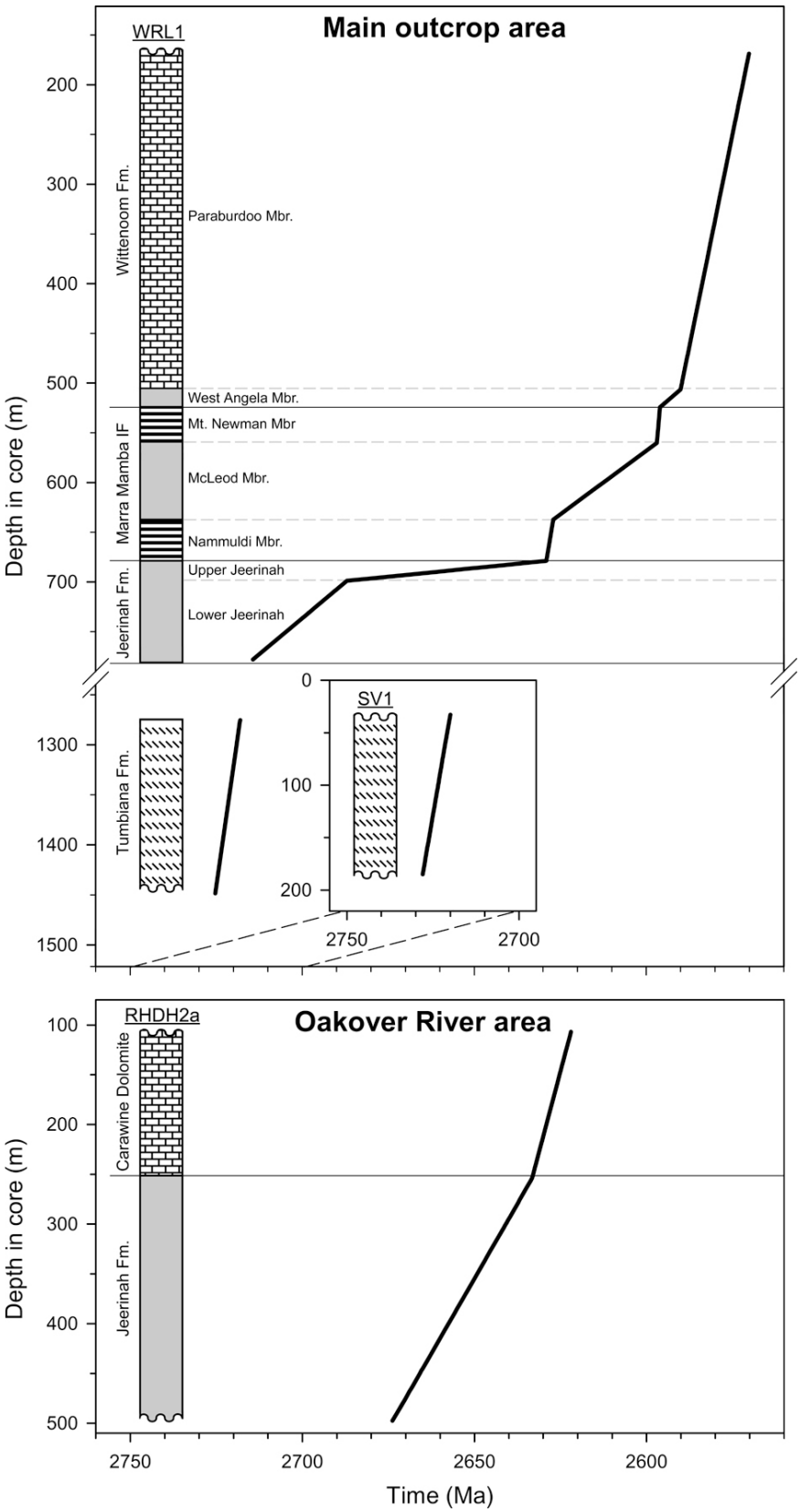

Fig. S1. Core depth versus calculated age for each core (note break in depth axis for core WRL1). Rates of deposition are equal to the slope of each line segment [similar to that of Trendall et al. (2004)].

S3. Fe isotope analyses

Approximately 10 mg of each rock powder was weighed into HCl-cleaned fused silica vials and heated in a furnace at 800–850 ºC overnight to remove carbonaceous matter. The ashed samples were digested in a 10-to-1 mixture of high purity 29 M HF and 14 M HNO_3 for three to five days. Following visual inspection to determine that all minerals were digested, each sample was dried down and the residues were brought up in high purity 8 M HCl overnight. Each sample was again visually inspected for undigested minerals, then dried and brought up in 5 mL of high purity 0.5 M HCl. Aliquots of each of these solutions were measured for total Fe content (see section S4.2) and an appropriate volume of each solution containing ~100 μg of Fe was prepared by purifying the Fe using ion exchange chromatography following the methods described by Beard and Johnson (1999).

Some analytical details are reported in section 2.4 of the main text. Fifty-eight samples were analyzed, and of these, seventeen were analyzed multiple times. Repeated measurements were of a single sample analyzed on different days, of replicate samples made from the same stock solution, or of replicate stock solutions made from the same rock powder (see Table S1). The average standard deviation (2 σ) for all of these repeated measurements is 0.06‰ (Table S1), which is essentially identical to that of pure standards.

Analytical accuracy was tested by producing artificial samples. A suite of samples that represented the entire range of compositions here analyzed was selected. During ion exchange chromatography of these samples, the acid used to purify each of these selected samples was collected and Fe of known isotopic composition was added. The resultant solutions were processed through the entire analytical procedure and Fe isotope compositions were measured. The results of these tests showed that our analytical methods produced accurate Fe isotope compositions.

S4. Geochemical and mineralogical analyses

Table S2 presents all of the geochemical data acquired during the course of this project, as well as isotope and whole-rock geochemical data collected by Yamaguchi et al. (2005), and carbon isotope data for extracted kerogen acquired by Eigenbrode and Freeman (2006).

S4.1 Whole-rock chemistry

Splits of rock powders were sent to Activation Laboratories (Actlabs) of Ancaster ON, Canada for whole-rock geochemical analyses. Because of a lack of sufficient material for some samples, not all samples were analyzed (see Table S2). The samples were analyzed for major oxides (16 samples), ferrous iron (FeO, 32 samples), total sulfur (S_{bulk}, 28 samples), total organic carbon (C_{org}, 23 samples), and carbonate carbon (C_{carb}, 31 samples) (Table S2).

Major oxides were analyzed by the standard fusion XRF technique of Norrish and Hutton (1969). Using this method, the detection limit for each oxide is ~0.01 wt. % except for MnO, which has a detection limit of ~0.001 wt. %. Ferrous iron was measured by titration following a method modified from that of Wilson (1955), which has a detection limit of ~0.01 wt. %. Total sulfur and organic carbon were measured by infrared elemental analysis with detection limits of ~0.01 and ~0.05 wt. %, respectively. Carbonate carbon was measured by coulometry with a detection limit of ~0.01 wt. %. Data quality was monitored by analyses of numerous standard reference materials (AC-E, AN-G, BE-N, BIR-1, BIR-1a, Calcium Carbonate, DNC-1, GBW 07113, IF-G, JSd-2, MICA-FE, MICA-Mg, NIST 694, SCH-1, SDO-1, SGR-1, SGR-1b, SY-4, W-2a, ZW-C).

Table S1. Iron isotope data collected during this study

	Sample ID[a]			Individual analyses				Grand averages			
	Core	Depth (m)	Repl.[b]	δ^{56}Fe	2 S.E.	δ^{57}Fe	2 S.E.	δ^{56}Fe	1 σ	δ^{57}Fe	1 σ
Main outcrop area											
Wittenoom Formation	WRL1-	178.3	1	-1.70	± 0.01	-2.46	± 0.02	-1.68	± 0.03	-2.44	± 0.03
			1	-1.66	± 0.03	-2.43	± 0.03				
	WRL1-	235.9A		-0.97	± 0.01	-1.40	± 0.02				
	WRL1-	235.9B		-1.35	± 0.02	-1.96	± 0.02				
	WRL1-	289.45	1	-1.44	± 0.02	-2.12	± 0.02	-1.44	± 0.00	-2.13	± 0.01
			1	-1.44	± 0.03	-2.13	± 0.02				
	WRL1-	298.28		-1.32	± 0.01	-1.97	± 0.02				
	WRL1-	338.57		-1.51	± 0.03	-2.20	± 0.03				
	WRL1-	376.4		-1.41	± 0.02	-2.05	± 0.02				
	WRL1-	472.2		-1.47	± 0.03	-2.17	± 0.03				
	WRL1-	499.01A		-0.23	± 0.02	-0.36	± 0.02				
	WRL1-	499.01B	1	-0.61	± 0.03	-0.93	± 0.02	-0.63	± 0.02	-0.96	± 0.02
			1	-0.64	± 0.03	-0.98	± 0.04				
			2	-0.62	± 0.04	-0.96	± 0.04				
	WRL1-	520.5	a	0.12	± 0.02	0.15	± 0.02	0.12	± 0.01	0.20	± 0.07
			b	0.13	± 0.03	0.24	± 0.03				
	WRL1-	520.6A	1	-0.20	± 0.02	-0.27	± 0.02	-0.17	± 0.03	-0.23	± 0.04
			2	-0.15	± 0.03	-0.22	± 0.03				
			2	-0.16	± 0.02	-0.19	± 0.02				
	WRL1-	520.6B	1	-0.54	± 0.02	-0.80	± 0.02	-0.57	± 0.04	-0.85	± 0.06
			1	-0.60	± 0.03	-0.89	± 0.03				
	WRL1-	524.05	1	-0.85	± 0.02	-1.25	± 0.02	-0.87	± 0.04	-1.27	± 0.04
			1	-0.86	± 0.04	-1.24	± 0.03				
			2	-0.91	± 0.02	-1.31	± 0.02				
Marra Mamba Iron Formation	WRL1-	544.8		-0.54	± 0.01	-0.78	± 0.02				
	WRL1-	560.2A		-0.57	± 0.02	-0.88	± 0.02				
	WRL1-	560.2B	1	-1.75	± 0.02	-2.54	± 0.02	-1.75	± 0.01	-2.54	± 0.00
			1	-1.74	± 0.03	-2.54	± 0.04				
	WRL1-	612.6		-0.17	± 0.03	-0.29	± 0.02				
	WRL1-	644.75		-0.82	± 0.02	-1.18	± 0.02				
	WRL1-	657.7	1	0.00	± 0.03	0.00	± 0.02	0.02	± 0.02	0.05	± 0.05
			1	0.03	± 0.02	0.08	± 0.02				
			1	0.04	± 0.04	0.08	± 0.02				
	WRL1-	659.5		-0.03	± 0.02	-0.05	± 0.02				
	WRL1-	673.6		0.36	± 0.04	0.55	± 0.02				
	WRL1-	678.75		-0.51	± 0.02	-0.76	± 0.02				
Jeerinah Fm.	WRL1-	678.95		-1.20	± 0.01	-1.75	± 0.01				
	WRL1-	679.9	1	-1.26	± 0.03	-1.86	± 0.02	-1.26	± 0.01	-1.87	± 0.01
			1	-1.27	± 0.03	-1.87	± 0.02				
			2	-1.27	± 0.02	-1.86	± 0.02				
			2	-1.26	± 0.03	-1.88	± 0.03				
	WRL1-	683.2		-1.05	± 0.03	-1.58	± 0.04				
	WRL1-	689.6		-1.06	± 0.02	-1.54	± 0.01				
	WRL1-	719.0		-0.63	± 0.02	-0.94	± 0.02				
	WRL1-	730.8	1	-0.63	± 0.02	-0.92	± 0.01	-0.63	± 0.03	-0.91	± 0.01
			1	-0.61	± 0.02	-0.90	± 0.02				
			1	-0.66	± 0.03	-0.92	± 0.02				
	WRL1-	731.05		-0.87	± 0.03	-1.32	± 0.03				
	WRL1-	731.33		-0.64	± 0.02	-0.92	± 0.02				

Table S1. (continued)

	Sample ID[a]		Individual analyses				Grand averages			
	Core Depth (m)	Repl.[b]	δ^{56}Fe	2 S.E.	δ^{57}Fe	2 S.E.	δ^{56}Fe	1 σ	δ^{57}Fe	1 σ
Tumbiana Fm.	SV1- 55.0	1	-0.02	± 0.02	-0.03	± 0.02	-0.05	± 0.05	-0.05	± 0.06
		1	-0.02	± 0.02	0.00	± 0.02				
		2	-0.10	± 0.02	-0.12	± 0.02				
	SV1- 55.3		0.14	± 0.02	0.21	± 0.02				
	SV1- 70.9		0.16	± 0.02	0.21	± 0.02				
	SV1- 117.0		-0.04	± 0.03	-0.08	± 0.03				
	SV1- 126.4		-0.04	± 0.02	0.00	± 0.02				
	SV1- 191.1		-0.25	± 0.02	-0.35	± 0.02				
Oakover River area										
Carawine Dolomite	RHDH2a- 125.1		-1.59	± 0.03	-2.33	± 0.03				
	RHDH2a- 135.6		-2.21	± 0.03	-3.26	± 0.02				
	RHDH2a- 136.0		-2.17	± 0.04	-3.18	± 0.02				
	RHDH2a- 141.0		-1.97	± 0.02	-2.90	± 0.03				
	RHDH2a- 141.7		-1.90	± 0.04	-2.77	± 0.03				
	RHDH2a- 147.6	1	-2.45	± 0.02	-3.63	± 0.02	-2.43	± 0.03	-3.59	± 0.05
		2	-2.42	± 0.02	-3.56	± 0.02				
	RHDH2a- 161.0		-2.42	± 0.03	-3.68	± 0.03				
	RHDH2a- 192.5		-1.40	± 0.05	-2.17	± 0.03				
	RHDH2a- 221.4		-1.81	± 0.02	-2.70	± 0.02				
	RHDH2a- 223.0		-1.76	± 0.04	-2.59	± 0.02				
	RHDH2a- 244.3		-0.65	± 0.03	-1.03	± 0.03				
	RHDH2a- 252.2	a	-1.34	± 0.02	-1.98	± 0.02	-1.30	± 0.03	-1.92	± 0.04
		b	-1.30	± 0.04	-1.91	± 0.04				
		c	-1.28	± 0.02	-1.87	± 0.02				
		c	-1.27	± 0.04	-1.91	± 0.02				
Jeerinah Fm.	RHDH2a- 285.3		-0.50	± 0.03	-0.70	± 0.03				
	RHDH2a- 296.9		-1.05	± 0.03	-1.52	± 0.03				
	RHDH2a- 299.3		-1.16	± 0.02	-1.70	± 0.02				
	RHDH2a- 333.5		0.36	± 0.02	0.58	± 0.02				
	RHDH2a- 337.03	a	-1.33	± 0.02	-1.97	± 0.02	-1.26	± 0.07	-1.84	± 0.13
		a	-1.25	± 0.02	-1.84	± 0.02				
		b	-1.19	± 0.04	-1.72	± 0.03				
	RHDH2a- 369.6		0.10	± 0.02	0.18	± 0.02				
	RHDH2a- 374.2	1	0.02	± 0.02	0.00	± 0.02	0.03	± 0.01	0.04	± 0.05
		1	0.04	± 0.04	0.07	± 0.03				
	RHDH2a- 447.2		-0.02	± 0.02	-0.04	± 0.02				
	RHDH2a- 496.1	1a	-0.09	± 0.02	-0.12	± 0.02	-0.06	± 0.03	-0.08	± 0.05
		1b	-0.08	± 0.04	-0.12	± 0.03				
		2	-0.05	± 0.02	-0.03	± 0.02				
		2	-0.03	± 0.03	-0.05	± 0.03				

[a] Uppercase letters refer to multiple samples cut from the same depth interval based on their apparent lithologies

[b] Numbers signify separate digestions of a signle rock powder, lowercase letters signify duplicate samples made from a single digestion. A repeated number or letter indicates a sample was analyzed multiple times.

Table S2. (See separate .xls file)

S4.2 Total iron contents

Total Fe contents were measured spectrophotometrically at UW-Madison on the same dissolved rock solutions used for Fe isotope analyses. A 38 μL aliquot of each sample was added to a 1.5 mL solution of 0.4 mM Ferrozine reagent and 288 mM hydroxylamine hydrochloride, and allowed to react overnight to ensure all Fe was reduced to. Absorbances were measured at 532 nm using a HACH spectrophotometer and converted to concentrations by use of standards.

S4.3 Reactive iron

Reactive iron measurements were made at UW-Madison following a protocol adapted from that of Leventhal and Taylor (1990) and Yamaguchi (2002). For each sample, 10 to 20 mg of powdered rock was digested in either 10 or 50 mL of 1 M HCl for 24 hours. We determined experimentally that digestion in these volumes of acid produce identical results. The samples were then centrifuged and the supernatant decanted. The residue was saved for carbonate content analyses, described below. Total and ferrous HCl-extractable iron content of the supernatant was measured spectrophotometrically. For total HCl-extractable Fe ($Fe_{T\text{-}HCl}$) measurements, each sample was analyzed under conditions identical to those used to measure total iron (described in section S4.2). The protocol for ferrous HCl-extractable Fe (Fe^{2+}_{HCl}) measurements was modified slightly and is based on that of Krishnamurti and Huang (1990). We added 50 μL of 432 mM ammonium fluoride to 38 μL of each sample, ensuring that they were well mixed, and then added 1.0 mL of a 2 mM solution of Ferrozine reagent. Ammonium fluoride will complex with ferric iron masking it from being complexed to the Ferrozine reagent. This step is critical because in the absence of ammonium floride the ferric iron–Ferrozine complex will undergo photoreduction prior to analysis leading to inaccurate measurements. Each sample was prepared individually and measured immediately.

S4.4 Carbonate contents

The remaining undigested residue from each reactive iron experiment was dried in a 55°C oven for ≥3 hours and then allowed to cool in a desiccator for ≥1.5 hours. The mass of the residue was measured and the difference between the original and final dry weights was considered to represent the mass of carbonate in each sample. We measured C_{carb} contents of four samples also analyzed for C_{carb} content by Actlabs, and the values agreed within 5 wt. %, and three of the four differed by less than 2 wt. % (see Table S2).

S4.5 X-ray diffraction

Mineral phase analyses were performed by X-ray diffraction at UW-Madison using a Scintag PADV X-ray diffractometer. Powdered samples were pressed into plastic sample holders and analyzed using Cu $K\alpha$ radiation (λ=1.5418Å). The parameters of each scan were identical; a 2θ angle of 5 to 70º, a step size of 0.2º, and a dwell time of 1 sec. Representative spectra are shown in Fig. S2 and have been normalized to the greatest peak intensity of each (without removing baselines). Mineral phases were identified by comparison of each spectrum with the JCPDS powder diffraction file (PDF-2).

S5. Determination of major Fe-bearing mineral phases

Whole-rock geochemical data in conjunction with XRD analyses of whole-rock powders and microscopic examination of core samples were used to determine the dominant Fe-bearing

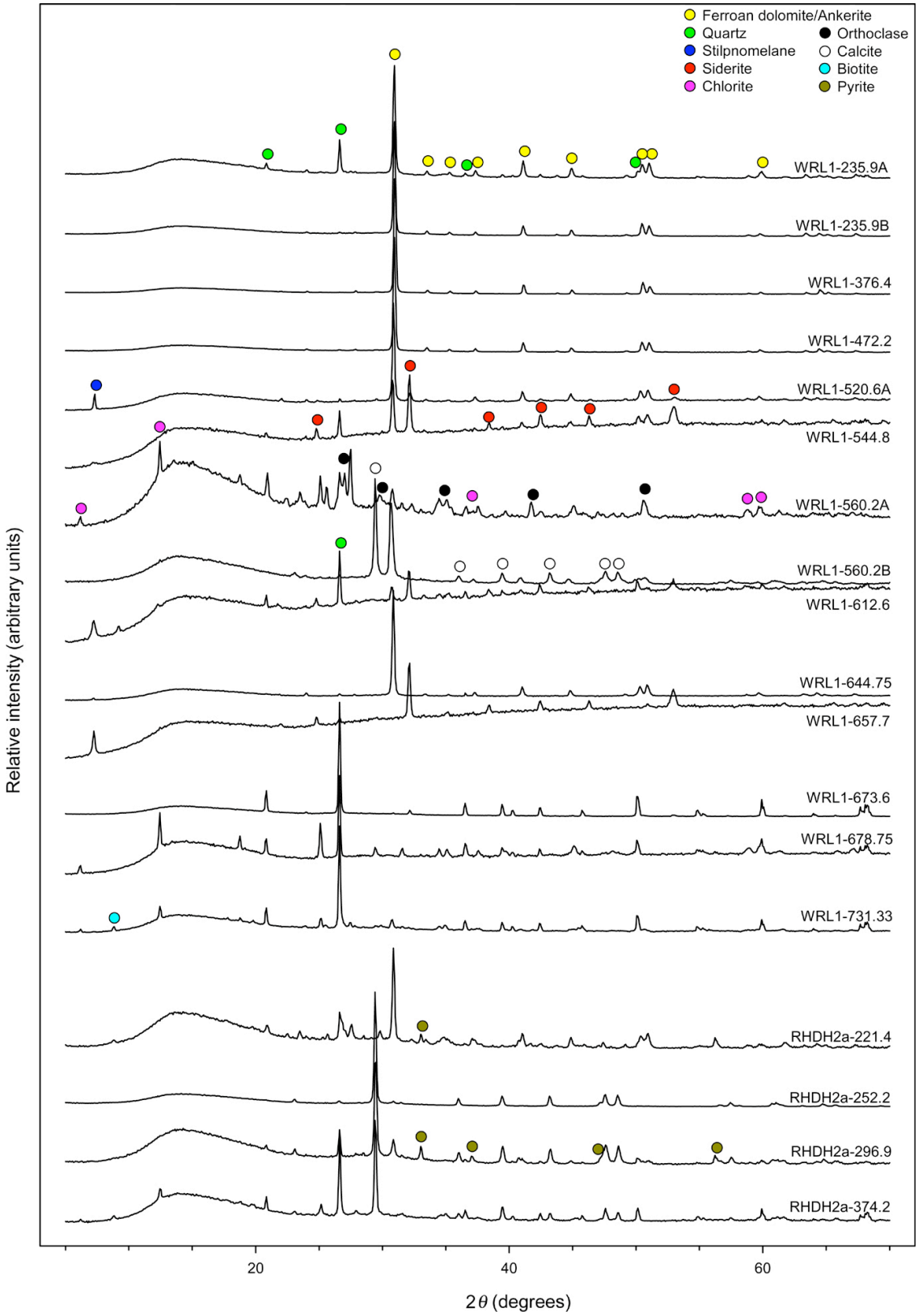

Fig. S2. XRD spectra of selected samples. Each spectrum has been normalized to the same maximum peak height with no baseline subtraction. Major peaks in the spectra of various mineral phases are indicated at their first occurrence from top to bottom in the figure. See Table S2 for a listing of major phases for each sample.

mineral phase or phases for each of the bulk samples analyzed here (Table S2). The possible Fe-bearing phases were grouped into three categories: Fe-carbonate ± oxides, pyrite ± oxides, and phyllosilicates ± others (Table S2). Fe-carbonates include the series of carbonates from ferroan dolomite to siderite. Phyllosilicates were not differentiated except for a few samples for which XRD patterns were acquired (Fig. S2).

Samples that have a high ratio of Fe^{2+} to total Fe (Fe_T) (Fig. S3A) must have a majority of their Fe in pyrite, carbonates, or phyllosilicates. The Fe balance controlled by pyrite is well constrained by Fe^{2+} and S contents based on the stoichiometry of FeS_2 and the assumption that all sulfur consists of pyrite. One sample (RHDH2a-333.5) had insufficient geochemical data to constrain Fe_{pyr}, but a reflected light microscopic examination of an off-cut of the sample revealed the presence of abundant pyrite (≥50% of the sample) and, thus, it is considered to have pyrite as its dominant Fe mineral. Figure S3B illustrates the distribution of Fe_{pyr} as a percent of Fe_T throughout the cores (see also Table S1).

Our interpretation of the abundance of Fe-carbonate in each sample is based largely on the amount of carbonate measured, either by coulometry or HCl extraction (Fig. S3C), and XRD analyses. Using major oxide content data from selected carbonate samples, we calculated the C_{carb} contribution of each significant carbonate cation (Ca, Mg, and Fe^{2+}, first subtracting the Fe^{2+} contribution from pyrite) to the total C_{carb} budget. When summed, these values matched very nearly the total C_{carb} values measured independently by coulometry, confirming the validity of the approach. From this we calculated an average stoichiometry of $Ca_{51}Mg_{46}Fe_3(CO_3)_{100}$ [standard deviations of 0.6 (Ca), 1.8 (Mg), and 1.9 (Fe)] for samples from the Wittenoom Formation and $Ca_{49}Mg_{42}Fe_9(CO_3)_{100}$ [standard deviations of 3.3 (Ca), 6.6 (Mg), and 8.0 (Fe)] for those of the Carawine Dolomite. Using these formulae and the measured C_{carb} values of each sample, we calculated the wt. % Fe in carbonate (Fe_{carb}) and then the approximate Fe_{carb}/Fe_T ratio (Table S2). For samples with low Fe_T contents, this proportion has a high uncertainty, so for these samples its use in determining the Fe-carbonate content was given lower weight. Carbonate-rich samples from the Marra Mamba Iron Formation for which major oxide data were collected were too variable in their compositions to produce a meaningful average carbonate stoichiometry. For the remaining Marra Mamba IF samples, Fe_{carb} contents were determined base on measured C_{carb} values and the stoichiometries of the carbonates (e.g., siderite and ferroan dolomite) as determined by XRD.

Calculations of Fe-carbonate content were confirmed using reactive Fe measurements. The Fe in carbonates is leached by the digestion procedure used here (see above), along with poorly crystalline Fe-oxides, which together comprise the HCl-extractable iron (Fe_{HCl}). Magnetite, pyrite, phyllosilicates, and other crystalline iron oxides are not dissolved. Iron carbonates will therefore have high values of $Fe_{T\text{-}HCl}/Fe_T$ (Fig. S3D), and high values of $Fe^{2+}{}_{HCl}/Fe_{T\text{-}HCl}$ (Fig. S3E), differentiating them from poorly crystalline iron oxides, which would have high $Fe_{T\text{-}HCl}/Fe_T$ ratios but low $Fe^{2+}{}_{HCl}/Fe_{T\text{-}HCl}$ ratios.

Phyllosilicates were interpreted to be the dominant Fe phase of the Fe budget based on a process of elimination, and considering Si and Al contents, where available. If the iron in the samples that have high Fe^{2+}/Fe_T ratios could not be accounted for by either pyrite or Fe-carbonate, it was assumed that Fe-bearing phyllosilicates comprised the major Fe repository. Phyllosilicates have very low solubility in HCl (Berner, 1970), so these determinations were confirmed by measurements of $Fe_{T\text{-}HCl}$. Additionally, XRD and/or microscopic observations were used to confirm these determinations.

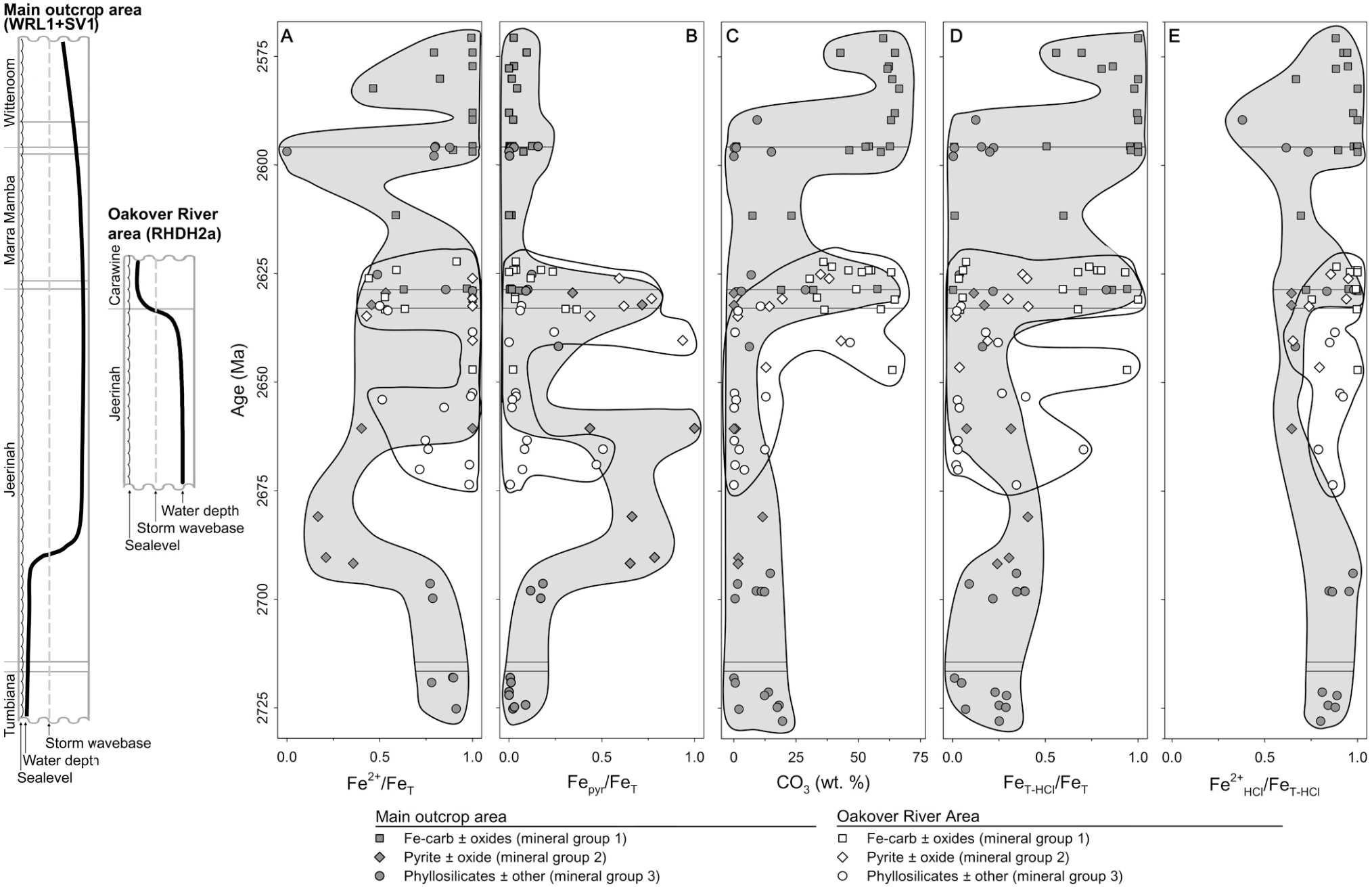

Fig. S3. Time profiles of ferrous iron (A), pyrite iron (B), carbonate (C), total HCl-reactive iron (D), and ferrous HCl-reactive iron (E) for each region of the Hamersley Province. Symbols for each sample indicate the dominant Fe-bearing mineral phases. Curves overlain on the stratigraphic columns (left-hand side) show relative water depths in each region of the province.

For samples that have a significant proportion of Fe^{3+} in their total iron budget, we concluded that either magnetite or some other Fe-oxide was present in significant amounts. An identification of magnetite was confirmed based on the gross presence or absence of magnetic particles in the rock powders of each sample.

S6. Paleoenvironmental redox conditions

The redox state of the various paleoenvironments recorded in the cores studied here is discussed in the main text of this paper, and additional constraints are provided in Figure S4. Euxinic environments generally have high levels of reduced sulfur and carbon, whereas oxidizing environments will have low levels of these elements. Suboxic or anoxic environments are distinguished from those that have euxinic conditions by high Fe^{2+}/Fe^{3+} ratios, but low sulfide contents. Figure S4 shows profiles of S (converted to pyrite abundance; Fig. S4A) and organic carbon (C_{org}; Fig. S4B) abundances in the Hamersley Province. Note the high levels of Fe_{pyr} and C_{org} in the Jeerinah Formation of the main outcrop area (deep-water) as well as in the Carawine Dolomite of the Oakover River area (shallow, but with restricted anoxic to suboxic settings).

The proportion of highly reactive Fe to total Fe (Fe_{HR}/Fe_T) and degree of pyritization (DOP) (Fig. S4C and D) are often used to determine the redox state of modern marine settings (e.g., Berner, 1970; Lyons and Severmann, 2006). Larger values of each of these, along with Fe_T/Al_T ratios, (Fig. 5 in main text) may indicate euxinic settings, but there are limitations to each proxy (see Lyons and Severmann (2006) for a detailed discussion). For example, note that the Wittenoom Formation has the most consistently high values of Fe_{HR}/Fe_T (~1, Fig. S4D), but all other proxies indicate it reflects an oxidizing and not euxinic environment (low S, C_{org}, and DOP).

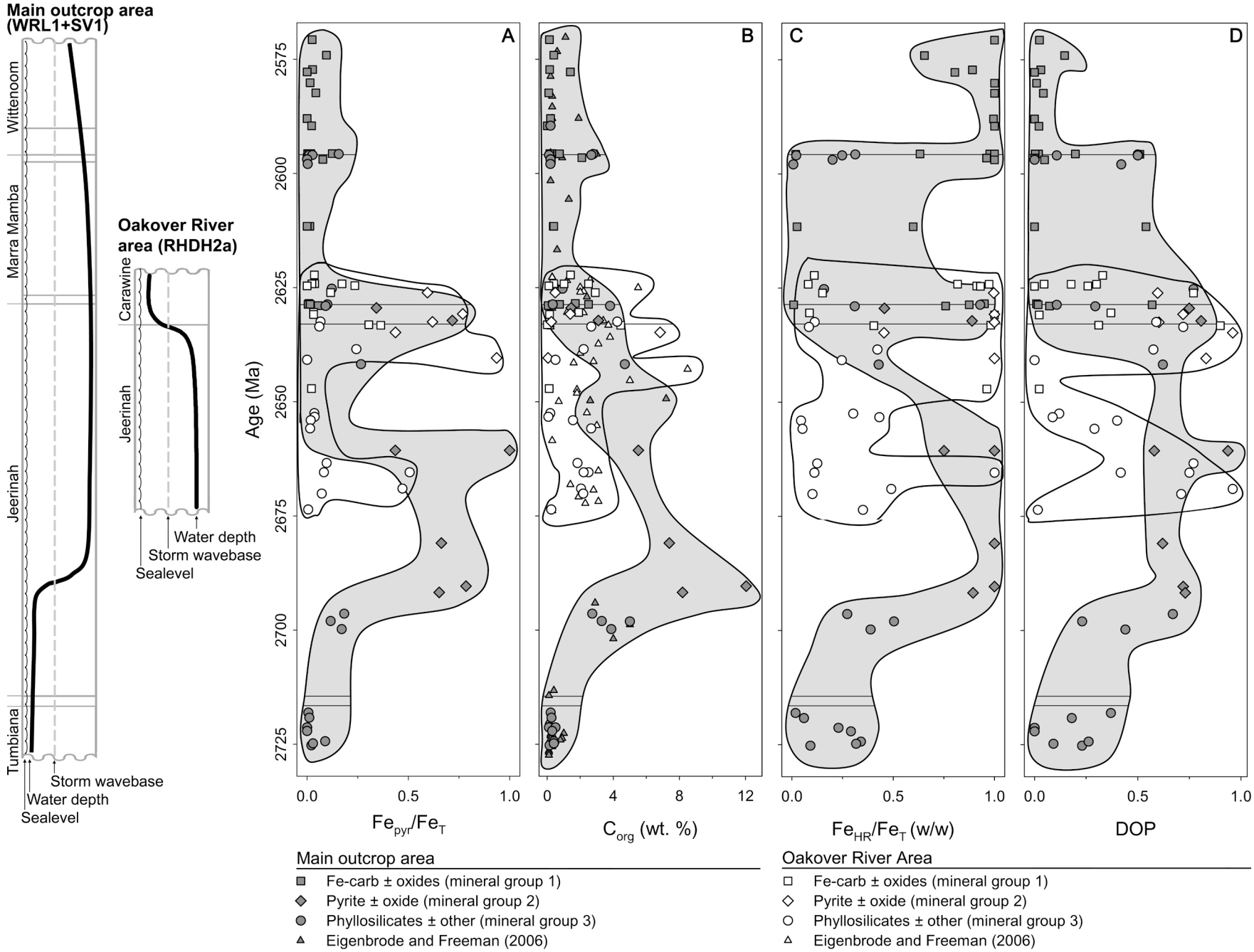

Fig. S4. Time profiles of pyrite iron (A), total organic carbon (B), highly reactive Fe to total Fe ratio (C), and degree of pyritization (D) for each region of the Hamersley Province. Symbols for each sample indicate the dominant Fe-bearing mineral phases. Water depth curves and symbols are the same as those used in Figure S3.

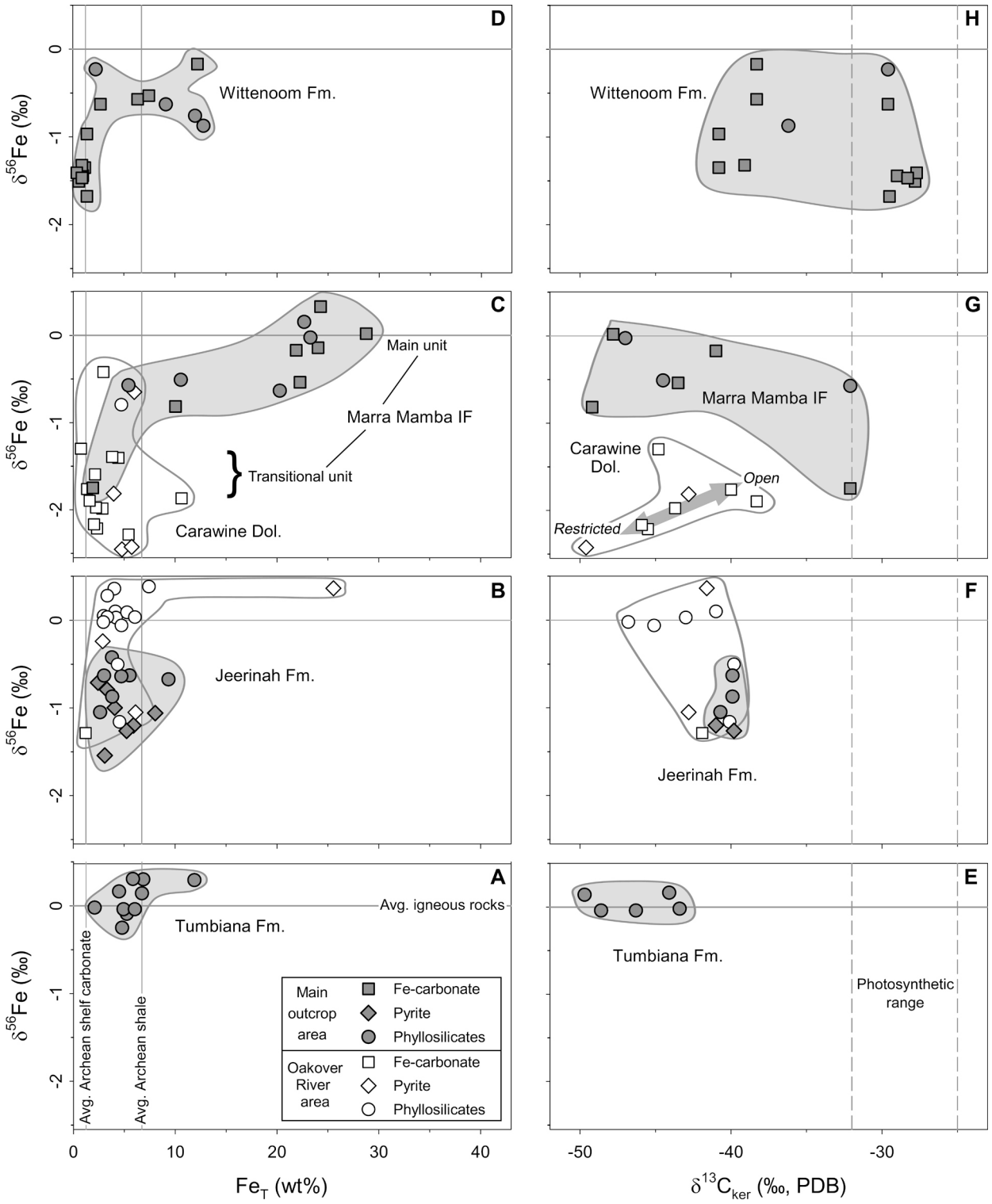

Fig. S5. Iron isotope composition versus wt. % total Fe content (A–D) and $\delta^{13}C_{ker}$ values grouped by geologic formation (E–H). Symbols used are the same as those in Figure S3. The horizontal reference line in each panel indicate the average $\delta^{56}Fe$ value of crustal rocks ($\delta^{56}Fe$ = 0‰). The vertical lines in parts A–D indicate the average Fe_T values of Archean shelf carbonates (Fe_T = 1.24 wt. %; Veizer et al., 1990) and Archean shales (Fe_T = 6.72 wt. %; Taylor and McLennan, 1985), and the dashed vertical lines in parts E–H indicate the range of carbon isotope fractionation produced by photosynthetic carbon fixation (cf. Fig. 4 in main text). In part G, the labels and double arrow indicate a trend of decreasing $\delta^{56}Fe$ and $\delta^{13}C$ values that correlate with samples being formed in open water environments versus those being formed in restricted environments (see main text for discussion). Samples WRL1-520.5 and WRL1-673.6 have been excluded because they have been altered by silicification.

References

Barley, M. E., Bekker, A., Krapez, B., 2005. Late Archean to early Paleoproterozoic global tectonics, environmental change and the rise of atmospheric oxygen. Earth Planet. Sci. Lett. 238, 156-171.

Beard, B. L. and Johnson, C. M., 1999. High precision iron isotope measurements of terrestrial and lunar materials. Geochim. Cosmochim. Acta. 63, 1653-1660.

Berner, R. A., 1970. Sedimentary pyrite formation. Am. J. Sci. 268, 1–23.

Buick, R., 1992. The antiquity of oxygenic photosynthesis: evidence from stromatolites in sulphate-deficient Archean lakes. Science. 255, 74–77.

Davy, R. and Hickman, A. H., 1988. The transition between the Hamersley and Fortescue groups as evidenced in a drill core. Geol. Surv. West. Aust. Report. 23, 85-97.

Eigenbrode, J. L. and Freeman, K. H., 2006. Late Archean rise of aerobic microbial ecosystems. Proc. Natl. Acad. Sci. U. S. A. 103, 15759-15764.

Hassler, S. W., Simonson, B. M., Sumner, D. Y., Murphy, M., 2005. Neoarchaean impact spherule layers in the Fortescue and Hamersley Groups, Western Australia: stratigraphic and depositional implications of re-correlation. Aust. J. Earth Sci. 52, 759-771.

Krishnamurti, G. S. R. and Huang, P. M., 1990. Spectrophotometric determination of Fe(II) with 2,4,6-tri(2'-pyridyl)-1,3,5-triazine in the presence of large quantities of Fe(III) and complexing ions. Talanta. 37, 745-748.

Leventhal, J. S. and Taylor, C., 1990. Comparison of methods to determine degree of pyritization. Geochim. Cosmochim. Acta. 54, 2621-2625.

Lyons, T. W. and Severmann, S., 2006. A critical look at iron paleoredox proxies: New insights from modern euxinic marine basins. Geochim. Cosmochim. Acta. 70, 5698–5722.

Meakins, A. L., 1987. CRA Exploration Pty. Ltd. final report on exploration completed within the Mulga Project area, Mt. Bruce 1:250 000 sheet, Pilbara region, Western Australia. Item 3458. Western Australia Geological Survey open file.

Morris, R. C., 1993. Genetic modelling for banded iron-formation of the Hamersley Group, Pilbara Craton, Western Australia; Archaean and early Proterozoic geology of the Pilbara region, Western Australia. Precambrian Res. 60, 243-286.

Norrish, K. and Hutton, J. T., 1969. An accurate x-ray spectrographic method for the analysis of a wide range of geological samples. Geochim. Cosmochim. Acta. 33, 431-453.

Rasmussen, B., Blake, T. S., Fletcher, I. R., 2005. U-Pb zircon age constraints on the Hamersley spherule beds: Evidence for a single 2.63 Ga Jeerinah-Carawine impact ejecta layer. Geology. 33, 725-728.

Richards, M. N., 1985. CRA Exploration Pty. Ltd. final report on exploration completed within exploration licenses Ripon Hills North 45/63, Ripon Hills South 45/64 and Gingarrigan Creek 45/65, Nullagine, S F 51-5, Western Australia. Item 2655. Western Australia Geological Survey open file.

Sakurai, R., Ito, M., Ueno, Y., Kitajima, K., Maruyama, S., 2005. Facies architecture and sequence-stratigraphic features of the Tumbiana Formation in the Pilbara Craton, northwestern Australia: Implications for depositional environments of oxygenic stromatolites during the Late Archean. Precambrian Res. 138, 255–273.

Simonson, B. M. and Carney, K. E., 1999. Roll-up structures: evidence of in situ microbial mats in late archean deep shelf environments. Palaios. 14, 13–24.

Simonson, B. M., Schubel, K. A., Hassler, S. W., 1993. Carbonate sedimentology of the Early Precambrian Hamersley Group of Western-Australia. Precambrian Res. 60, 287-335.

Taylor, S.R., McLennan, S.M., 1985. The Continental Crust: its Composition and Evolution. Blackwell Scientific Publications, Oxford.

Thorne, A.M., Trendall, A.F., 2001. Geology of the Fortescue Group, Pilbara Craton, Western Australia. Geological Survey of Western Australia, Bulletin 144. 249 pp.
Trendall, A.F., Blockley, J.G., 1970. The iron formations of the Precambrian Hamersley Group, Western Australia. Geological Survey of Western Australia, Bulletin 119. 366 pp.
Trendall, A. F., Compston, W., Nelson, D. R., De Laeter, J. R., Bennett, V. C., 2004. SHRIMP zircon ages constraining the depositional chronology of the Hamersley Group, Western Australia. Aust. J. Earth Sci. 51, 621–644.
Veizer, J., Clayton, R. N., Hinton, R. W., von Brunn, V., Mason, T. R., Buck, S. G., Hoefs, J., 1990. Geochemistry of Precambrian carbonates: 3-shelf seas and non-marine environments of the Archean. Geochim. Cosmochim. Acta. 54, 2717-2729.
Williams, I.R., 2007. Geology of the Yilgalong 1:100,000 sheet, explanatory notes. Geological Survey of Western Australia. 45 pp.
Wilson, A. D., 1955. A new method for the determination of ferrous iron in rocks and minerals. Bull. Geol. Sur. Gt. Britain. 9, 56-58.
Yamaguchi, K. E., 2002. Geochemistry of Archean-Paleoproterozoic black shales: the early evolution of the atmosphere, oceans, and biosphere. Ph.D. thesis, Pennsylvania State University. 485 pp.
Yamaguchi, K. E., Johnson, C. M., Beard, B. L., Ohmoto, H., 2005. Biogeochemical cycling of iron in the Archean–Paleoproterozoic Earth: constraints from iron isotope variations in sedimentary rocks from the Kaapvaal and Pilbara Cratons. Chem. Geol. 218, 135–169.